Noise characterization of a 512 x 16 SPAD line sensor for time-resolved spectroscopy applications

Noise characterization of a 512 x 16 SPAD line sensor for time-resolved spectroscopy applications

Neil Finlayson, Andrea Usai, Ahmet T. Erdogan, Robert K. Henderson

School of Engineering, Institute for Integrated Micro and Nano Systems, University of Edinburgh, King's Buildings, Alexander Crum Brown Road, Edinburgh EH9 3FF, UK

ABSTRACT

Time-resolved spectroscopy in the presence of noise is challenging. We have developed a new 512 pixel line sensor with 16 single-photon-avalanche (SPAD) detectors per pixel and ultrafast in-pixel time-correlated single photon counting (TCSPC) histogramming for such applications. SPADs are near shot noise limited detectors but we are still faced with the problem of high dark count rate (DCR) SPADs. The noisiest SPADs can be switched off to optimise signal-to-noise-ratios (SNR) at the expense of longer acquisition/exposure times than would be possible if more SPADs were exploited. Here we present detailed noise characterization of our array. We build a DCR map for the sensor and demonstrate the effect of switching off the noisiest SPADs in each pixel. 24% percent of SPADs in the array are measured to have DCR in excess of 1kHz, while the best SPAD selection per pixel reduces DCR to 53+/-7Hz across the entire array. We demonstrate that selection of the lowest DCR SPAD in each pixel leads to the emergence of sparse spatial sampling noise in the sensor.

Keywords: SPAD, Single Photon Counting, TCSPC, Histogram, Spectroscopy, Fluorescence lifetime, Raman, CMOS, sparse sampling noise, DCR.

1. INTRODUCTION

Spectrometers based on time-resolving single photon avalanche diode (SPAD) detectors are used for time correlated single photon counting (TCSPC) spectroscopy and imaging[1] where photon numbers are measured as a function of wavelength and time, with rich applications in nanosecond-scale fluorescence lifetime microscopy, Raman sensing, Forster resonance energy transfer (FRET) sensing and bio-medical confocal imaging of cells.[2] The impact of detection noise and other signal distortions on such spectrometers is of considerable interest,[3] in terms of optimising signal-to-noise ratios (SNR). Sources of spectrometer noise and distortion include shot noise, dark count noise, pile-up distortion and optical aberrations. In this paper we highlight another noise source - sparse spatial sampling noise arising from under-sampling in the spectrometer focal plane.

Line sensors are key components in highly parallel TCSPC spectrometer architectures.[1] A diffraction grating and focusing lens are used to split light in the spectrometer into individual wavelengths dispersed across the line sensor pixel array. Line sensors are often fabricated using two-dimensional arrays of CMOS SPAD detectors such that multiple SPADs are dedicated to each pixel to increase sensitivity, photon detection rate and to reduce dead-time.[4]

TCSPC pixels typically incorporate photon time-stamp processing logic based on time-to-digital converters (TDC). Recently we developed a line sensor which supplements the generation of TCSPC time-codes with on-chip histogramming functionality for each pixel, greatly increasing sensor throughput.[5] The line sensor has 512 pixels with 16 SPAD detectors per pixel integrated with in-pixel TCSPC histogramming for time-resolved spectroscopic and imaging applications. The sensor opens up new applications in hyperspectral scanning systems in microscopy, endoscopy and aerial monitoring as well as new modalities in ring-down, fluorescence lifetime and Raman spectroscopies.[1,3,6,7]

SPADs are near shot noise limited detectors but display dark count rate (DCR) events associated with thermal generation of free-carriers arising from crystal defects and/or impurities. High-noise SPADs can be switched off[8] and this approach can be used to optimise signal-to-noise ratios at the expense of longer acquisition/exposure times than would be possible if more SPADs were exploited. Here we present detailed noise characterization of our line sensor. We build a DCR map for the sensor and demonstrate the effect of switching off the noisy SPADs in each pixel using a variety of SPAD

activation matrices. We investigate the effect of a 'best SPAD' SNR-optimisation strategy on the single-photon counting (SPC) and on-chip TCSPC histogramming operating modes of the sensor.

A new phenomenon is presented where attempts to reduce temporal DCR noise through SPAD selection can lead to sparse spatial sampling of the optical field and a consequent increase of spatial sampling noise. Sparse sampling noise arises from a stochastic positional distribution of activated SPADs, and is particularly problematic in the near neighbourhood of the spectrometer focal plane. We compare the effects of several SPAD activation matrices on spectrometer performance. The high signal throughput offered by our line sensor enables us to perform richly detailed characterisation of the effects of sparse sampling noise, DCR and pile-up.

2. NOISE AND DISTORTIONS

Optical signals in fluorescence lifetime spectroscopy are subject to various kinds of distortion.

2.1 Dark Counts

Dark count events are spurious avalanches which can occur due to thermally generated carriers or band-to-band electron tunnelling. DCR arises from process imperfections and can vary considerably from one SPAD to the next. High DCR SPADs can be selectively switched off so that only low DCR SPADs are activated.

2.2 Spatial Sampling Noise

The physical dimension of a single SPAD is on the order of several μm, a pixel on the order of a hundred μm and our line sensor array is 12.5 mm in width. In a spectrometer, optical beams are focused to very small volumes on the order of the sensor dimensions. Detection of such beams turns out to be impacted considerably by the choice of SPAD activation matrix (spatial patterns of switched-on SPADs). If too few SPADs are activated in areas of greatly changing field intensity (e.g. at the focal plane of the spectrometer lens) attempts to mitigate temporal DCR in the SPAD array can be thwarted by the emergence of sparse spatial sampling noise.

2.3 Pile-up

In 'classic' pile-up TCSPC histogram bins corresponding to time slots for measuring individual fluorescent events are unable to record a second photon in a single signal period.[2] Consequently, the second photon is lost. If the number of counts in a given time slot, i, is N_i and the total number of excitation cycles is E, a photon in time-slot i cannot trigger the TDC if a photon in a previous time-slot, $j < i$, has already triggered the TDC. The effective number of excitation cycles available to time-slot i is consequently reduced as shown in Eq (1)

$$E_i = E - \sum_{j=1}^{i-1} N_j \tag{1}$$

This leads to a signal distortion in the measured fluorescence decay leading to a reduction in measured lifetime τ_{meas} compared with the true value τ as given by

$$\tau_{meas} = \tau \frac{e^P - 1}{Pe^P} \tag{2}$$

where P is the sum of the probabilities Pj, that a photon appears at a time corresponding to time-slot j in one signal period. P can be considered as the average number of photons per signal period.

If E is large (MHz repetition rates with exposure times of a few seconds) the reduction in effective number of excitation cycles for photon events occurring in later time-slots is insignificant. However at kHz laser repetition rates the signal distortion can be substantial.

2.4 Optical Aberrations

Further complicating factors are spectrometer aberration arising from the collimating lens, the diffraction grating and the focusing lens. These aberrations have the effect of introducing spatial distortions into the optical field.

3. LINE SENSOR

The spectrometer sensor is a 16.5 giga-events/s 1024 × 8 SPAD Line Sensor implemented in CMOS with 23.78um pixel pitch.[5] Each pixel incorporates a 32 bin histogramming time-to-digital converter with zoomable time ranges from 1.6ns to 204.8ns. The sensor can operate in single photon counting (SPC) mode with a throughput of 65 giga-events/s, time-correlated single photon counting (TCSPC) mode (194 million-events/s) or histogramming mode (16.5 giga-events/s). A bottleneck is usually implied by readout of per pixel time-events from TDCs to implement TCSPC off-chip. We employ on-chip histogramming at a per-pixel level achieving up to two orders of increase in SPAD photon processing rates enabling fast scanning or low I/O power time-resolved spectroscopic imaging. As a result we are able to acquire time-resolved spectral data at very high rates, enabling rapid production of rich detailed TCSPC spectroscopic datasets.

4. SPECTROMETER MODEL

A simple model for the spectrometer incorporates a diffraction grating, a focusing lens and the line sensor. Detection occurs at the sensor array as shown in Fig. 1 (a).

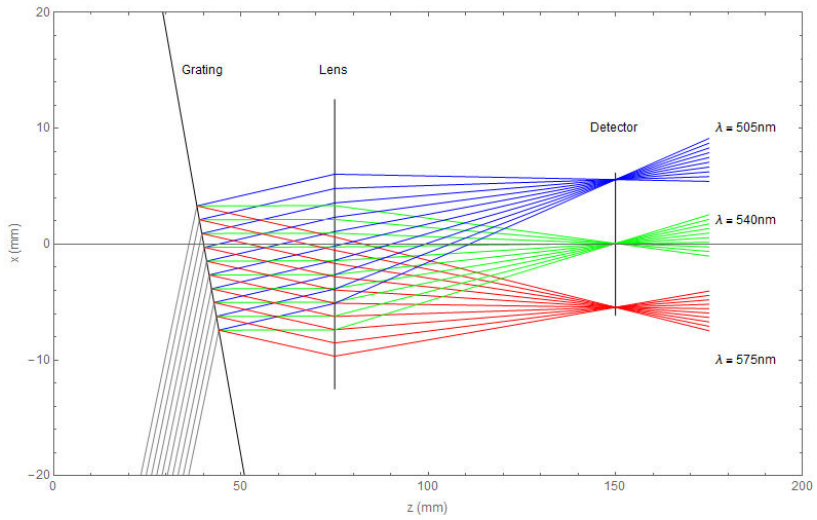

(a)

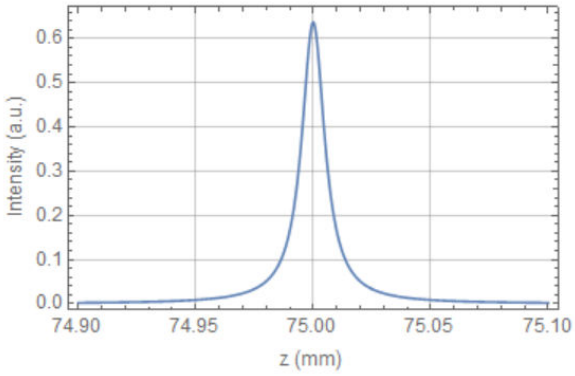

(b)

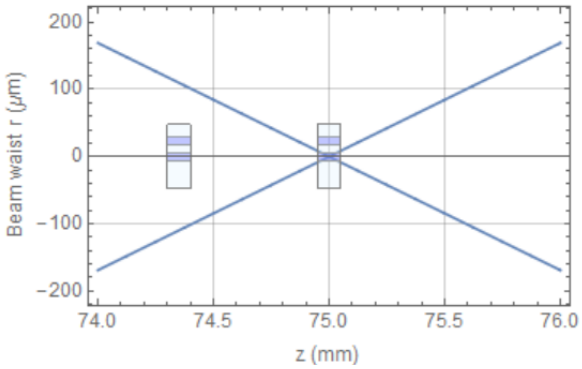

(c)

Figure 1. Line sensor placement. (a) Ray tracing model. (b) Intensity as a function of longitudinal distance z from lens, (c) Detector positions relative to beam waist (i) sensor array height less than beam waist (ii) sensor array height greater than beam waist (i.e. at focal plane).

Signals in the neighbourhood of the focal plane can be investigated by x-y-z-movement using translation stages. The detected spectral region can be shifted by 35nm by a 6mm transverse movement of the detector array in the horizontal x-

direction. The optical intensity rises rapidly at the focus as shown schematically in Fig. 1(b). When placed at the focal plane of the spectrometer lens the line sensor height can exceed the optical beam waist as shown in Fig 1 (c). Longitudinal z-axis displacement from the focal plane is then required to ensure that the optical beam covers the entire sensor array.

4.1 SPAD Activation Matrix

The sensor incorporates per-SPAD activation circuitry allowing high DCR SPADs to be disabled. Each pixel has 2 columns of 8 SPADs with properties optimised for the blue region of the spectrum with a further 2x8 SPAD array optimised for the red region of the spectrum. Pixel SPADs are pre-programmed before acquisition. The SPAD activation matrices shown in Fig. 2 are used to investigate various forms of signal distortion. (a) **Activation Matrix A:** all SPADs on including those with high DCR (b) **Activation Matrix B:** single SPAD row (2 SPADs per pixel), (c) **Activation Matrix B:** single SPAD per pixel having the lowest DCR, (d) **Activation Matrix D:** 4 best DCR SPADs per pixel by selecting one SPAD from each pair of adjoining rows. Every pixel in the array can be programmed with a custom activation matrix.

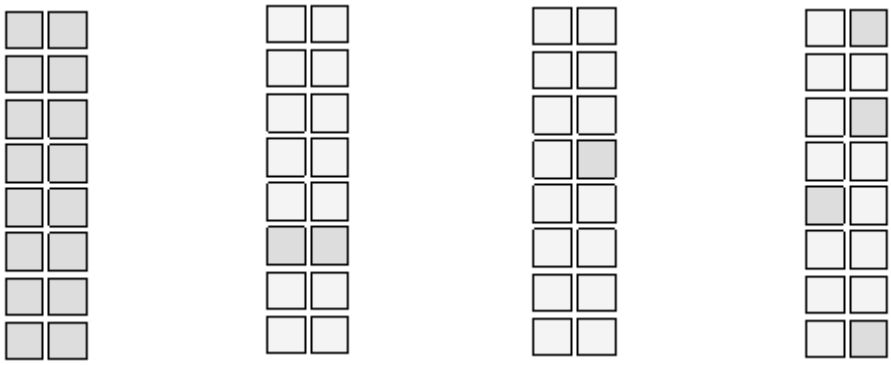

(a) (b) (c) (d)

Figure 2. Example SPAD activation matrices for a single pixel (a) all SPADs, (b) single SPAD row, (c) single SPAD, (d) one low DCR SPAD selected from each pair of adjoining rows.

5. EXPERIMENTAL METHOD AND RESULTS

The effects of various spectrometer noise sources and distortions are investigated with a white light source and a 4kHz repetition rate laser where DCR on the order of kHz is a particular problem.

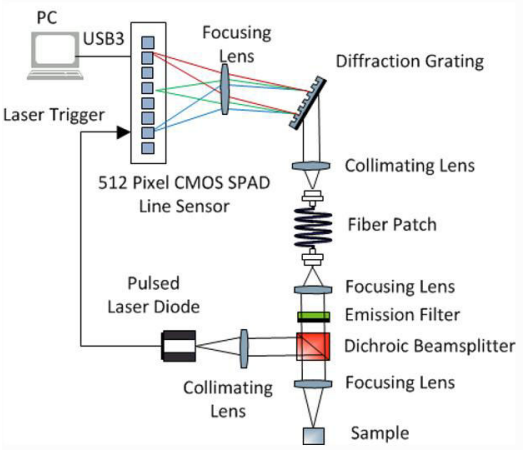

Figure 3. The spectrometer.

Single photon counting tests are carried out predominantly with white light illuminating the diffraction grating. For TCSPC investigations an epi-fluorescence setup is used as shown in Fig. 3. Fluorescence is collected from a cuvette filled with Rhodamine B. The fluorescence is focused into a multimode fiber and relayed to a spectrograph consisting of dispersive optics with CMOS SPAD line sensor placed in focus. The sample is illuminated by a TeemPhotonics STG-03E 532 nm pulsed laser diode operating at a 4 kHz repetition rate. Dichroic filters were used to separate illumination from fluorescence. Spectrograph diffraction was accomplished using a volume phase holographic grating (1200 lp/mm at 600nm, Wasatch Photonics) with collimating and focusing lens optimized for efficiency and spectral resolution.

5.1 Dark Count Characterisation

DCR is measured in dark conditions in SPC mode. Each SPAD is turned on in succession in each pixel with an exposure of 1s. This is followed by ranking SPADs in each pixel based on their DCR. Fig. 4 shows DCR results for selected SPADs per pixel (i.e. 1st best, 11th best and 16th best). In overall, 24% percent of SPADs in the sensor are measured to have DCR in excess of 1kHz, while selection of the lowest noise SPAD in each pixel reduces DCR to 53+/-7Hz across the entire pixel array.

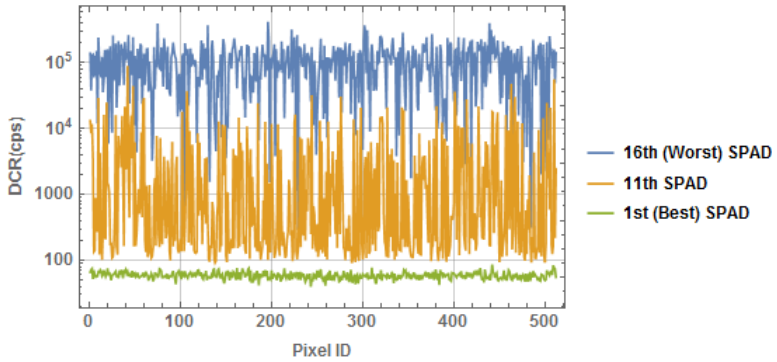

Figure 4. Measured DCR across the pixel array for the 1st best SPAD, 11th best SPAD and 16th best (i.e. worst) SPAD.

5.2 SPC Mode - White light

5.2.3 Activation Matrix A: All SPADs on

When all SPADs are activated we see strong evidence of DCR in SPC mode, as shown in Fig. 5.

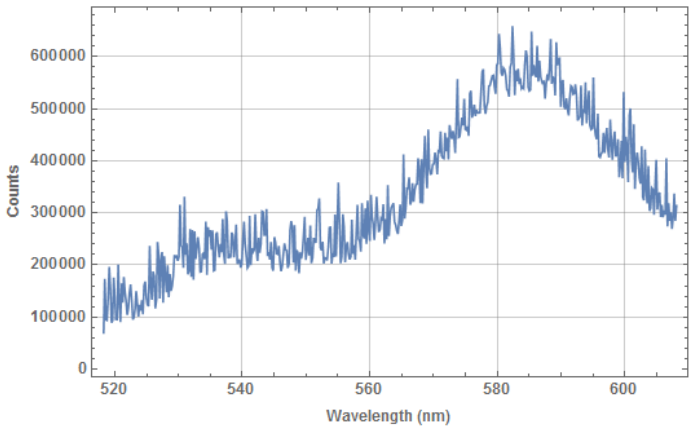

Figure 5. White light signal at the focal plane with all 16 SPADs on. Strong DCR in evidence.

5.2.1 Activation Matrix B: Single SPAD row, 2 SPADs per pixel

In Fig. 6 we demonstrate the use of **Activation Matrix B** in SPC mode with a white light source (Brunel Cold Light Source). Each row of the sensor array is successively activated to build a composite picture of the wave-front at the focal

plane. The beam is tightly focused, with a line focus confined to an area less than the area of the sensor (12.5mm × 95μm). The white light source has an uneven spectral distribution, so that there is some variation in field intensity in the horizontal direction. In addition we observe strong distortion of the field (field curvature) arising from optical aberrations and misalignment in the system. Field curvature and other aberrations can be overcome in principle through optical component selection and good alignment. Tightly focused beams are desirable characteristics in general which optimise the photon number and spectral resolution. As will be shown in the next section, tight focusing of the optical field and field curvature in the focal plane can lead to serious signal distortions if the field is spatially under-sampled i.e. too few detectors are activated in the focal plane.

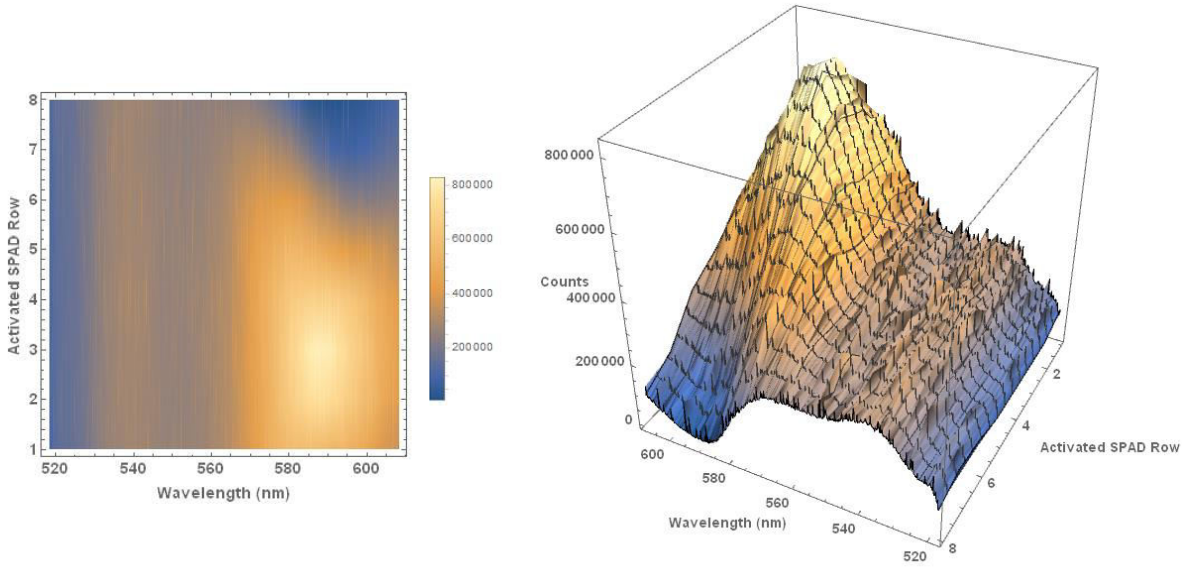

Figure 6. White light signal measured in focal plane by each SPAD row. Strong field curvature is in evidence in the 560-610nm spectral region

5.2.2 Activation Matrix C: Single SPAD per pixel with lowest DCR

An ostensible route to achieving the best possible SNR is to select the lowest DCR SPAD in each pixel. The first disadvantage of this scheme is that turning off additional SPADs lowers overall sensitivity and increases exposure times. A more subtle problem is sparse sampling noise arising from the position distribution of activated SPADs. Fig. 7 shows the spatial distribution of lowest DCR SPADs. When Activation Matrix C is used to activate the lowest DCR SPAD in each pixel, sampling of the optical field in the region of the focus is very sparse as shown in Fig. 7(b).

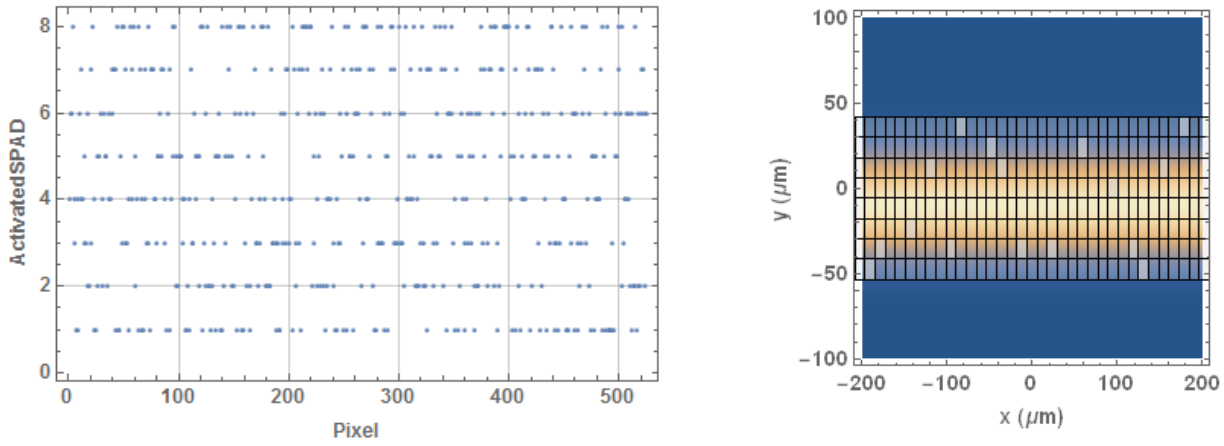

(a) (b)

Figure 7. Activation Matrix for best DCR SPAD. (a) 1 SPAD activated per pixel – 'sparse sampling algorithm'. (b) Close-up model of SPAD distribution in the focal plane. Some SPADs lie outside the beam waist.

Signals obtained with Activation Matrix C are compared with those from Activation Matrix B in Fig. 8. Activation Matrix B signals from each row of SPADs are re-plotted in Fig. 8(a), showing high DCR spikes and the effect of optical aberrations – strong field curvature occurs in the 560-610 nm spectral region, and the signals from individual rows of SPADs diverge considerably as a result.

DCR is lowered with Activation Matrix C but an intense distortion of the measured optical signal at the focal plane is observed in the 560-610 nm spectral range, as shown in Fig. 8(b). This arises as a result of sparse sampling, which is greatly intensified in regions where the optical field intensity is changing most rapidly. In the wavelength region between 520nm and 560nm the rate of change of the optical field intensity is not great so the signal can be sampled sparsely without introducing severe sampling noise. In the region from 560nm to 610nm the field curvature is much greater and under-sampling leading to sampling noise/distortion is more evident.

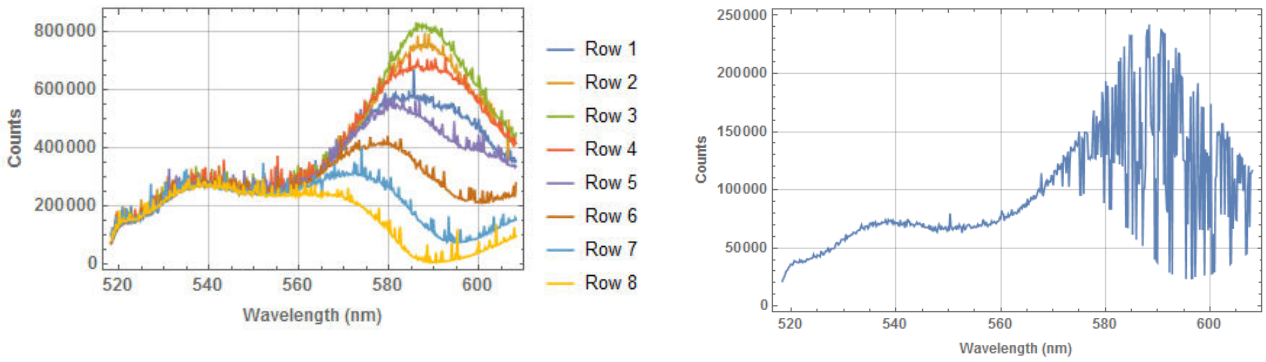

(a) (b)

Figure 8. (a) Activation Matrix B where signals from each row of SPADs are plotted, showing high DCR spikes. The effects of field curvature lead to considerable diverge in the individual row signals in the 560-610nm region. (b) Activation Matrix C where white light signal measured in focal plane by single lowest DCR SPAD activated. Sparse sampling leads to strong spatial sampling noise components in the region of greatest rate of change of the optical field. Signals exhibit low DCR but high sparse spatial sampling distortion which traces out the envelope of the Matrix B signals.

In Fig. 9 we translate the detector array in the longitudinal z-direction. The detector is moved from -5mm to +13mm where 0mm denotes the focal plane - 75 different positions in all, in steps of 250μm. Sparse sampling noise is strongly in evidence. Note that the noise is pixel specific – it is *invariant* as we move in the z-direction.

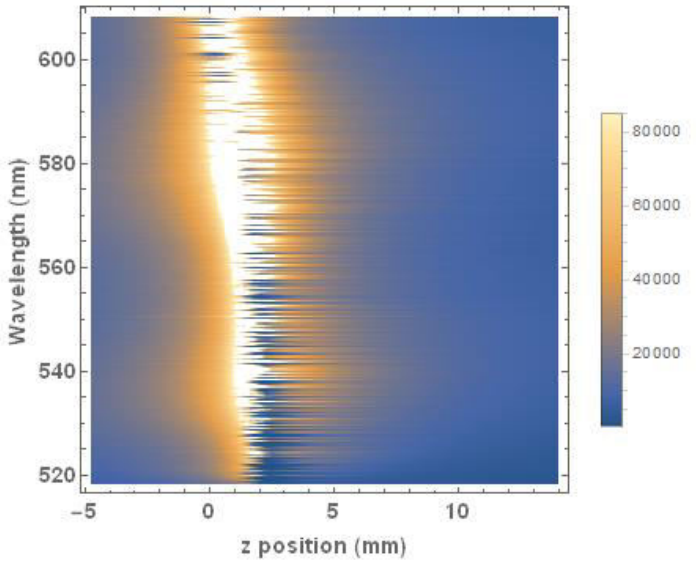

Figure 9 Density plot of sensor signals with sparse sampling/low DCR (1 SPAD per pixel activated). White light signal with sparse sampling noise strongly in evidence. Detector array is translated longitudinally through the focus to 75 positions in steps of 250µm.

5.2.4 Activation Matrix D: 4 SPADs per pixel with best of 4 in contiguous rows

A trade-off is clearly desirable to mitigate the effects of both DCR and sparse sampling noise. Sparse spatial sampling can be mitigated by relaxing the DCR constraints and switching on more SPADs to sample more densely across the wave-front in the focal plane. An example is shown in Fig. 10 where, for each pixel, we activate the lowest DCR SPAD in pairs of adjacent rows resulting in four SPADs turned on in each pixel with more even spatial distribution than exhibited by Activation Matrix C.

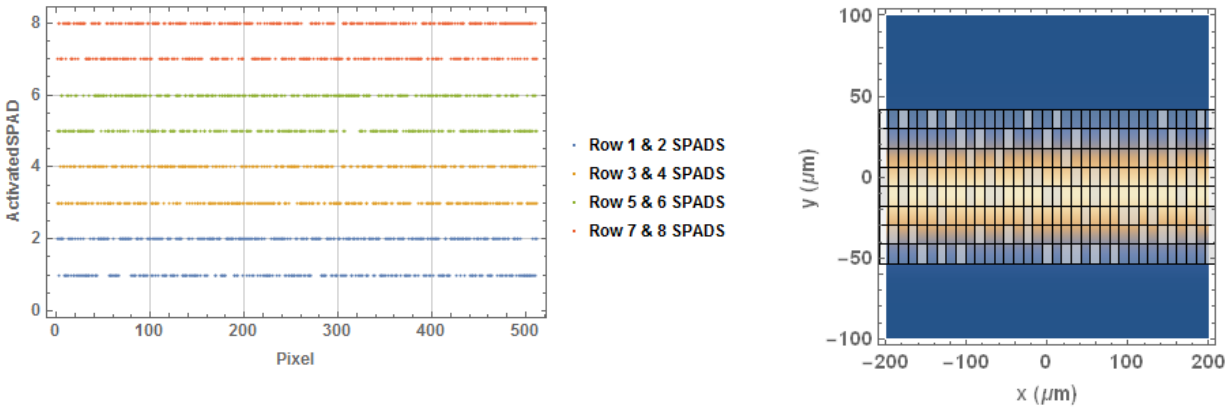

(a) (b)

Figure 10. Activation Matrix D for best DCR SPADs in adjacent rows. (a) 4 SPADs activated per pixel. Sampling is much more uniform than in the sparse sampling case (Fig. 7(a)). (b) Close-up model of SPAD distribution in the focal plane. The optical field region inside the beam waist is more densely sampled.

The effect of Activation Matrix D is dramatic. Both DCR and sparse sampling noise are greatly reduced as shown in Fig. 11.

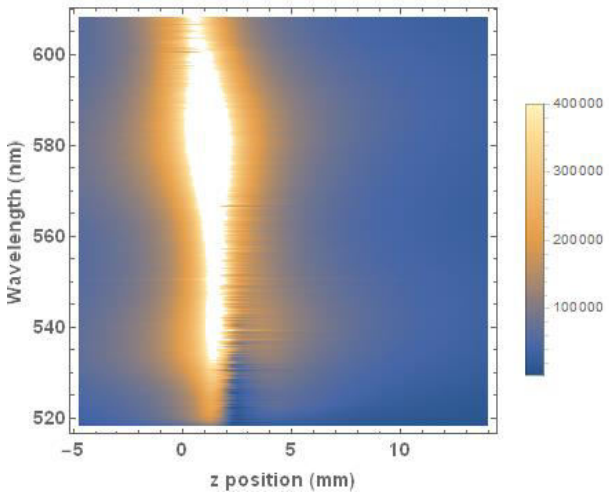

Figure 11. Density plot of sensor signals with 4 SPADs per pixel activated. Sparse sampling noise greatly reduced.

In Fig. 12 we plot the detector signal against longitudinal position for 2 specific pixels. In Fig. 12(a) where only 1 SPAD per pixel is activated the activated SPAD in pixel 2 is located near the centre of the optical wave-front beam waist. In pixel 5, the activated SPAD is located outside the waist and is subject to severe sparse sampling distortion as the focal plane is traversed as a result. Fig. 12 (b) demonstrates that activating 4 SPADs in Pixel 5 removes the distortion. In addition we also get more counts over the Activation Matrix B case because we have 4 SPADs switched on as opposed to 1.

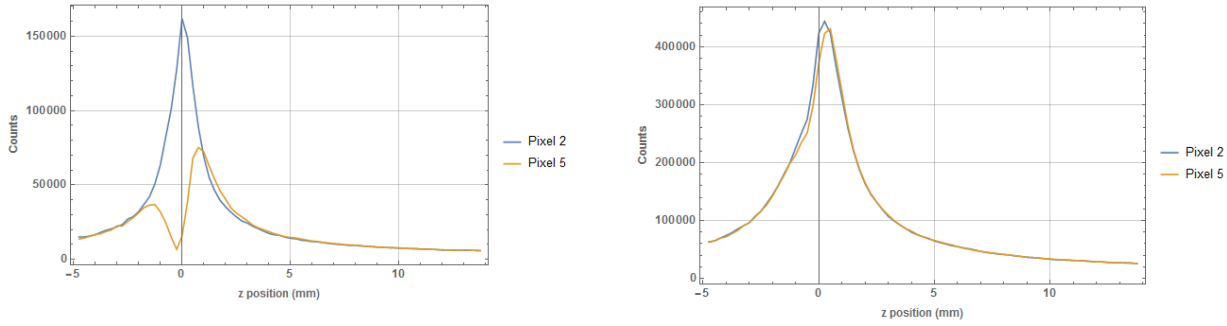

(a) (b)

Figure 10. Signal variation with longitudinal position for two pixels. (a) With 1 SPAD activated (Activation Matrix C) Pixel 2 SPAD is located near the centre of the optical wave-front beam waist. Pixel 5 SPAD is located outside the waist and is subject to sparse sampling noise. (b) With 4 SPADs activated (Activation Matrix D) Improved positional distribution of SPADs leads to disappearance of sparse sampling noise in pixel 5.

6.3 On-chip TCSPC Histogramming Mode

Finally we investigate the influence of signal distortions arising from these Activation Matrices on fluorescence lifetime measurements. We deploy the sensor in TCSPC histogramming mode. A typical time-resolved spectrum for Rhodamine B is shown in Fig. 11, where the vertical counts axis is shown on a log scale. Lifetimes are calculated through a linear fitting procedure for each of 512 spectral positions.

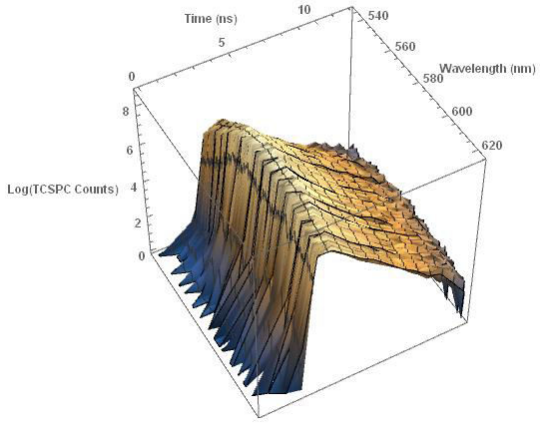

Figure 11 Time-resolved spectrum for Rhodamine B. Note that vertical axis is on a log scale.

The effects of Activation Matrix C (1 lowest-DCR SPAD per pixel) and Activation Matrix D (4 lowest-DCR SPADs per pixel activated in adjacent row pairs) on fluorescence lifetime are contrasted in Fig. 12. Rhodamine fluorescence lifetimes detected in histogramming mode at 512 wavelengths x 75 spatial positions in the neighbourhood of the focal plane of the spectrometer lens are shown. In Fig. 12 (a) 1 lowest-DCR SPAD is activated. There is some evidence of sparse sampling noise. The blue regions in the vicinity of the focus are affected by pile-up owing to low repetition rate and exposure times. The 1 SPAD case shows a near flat lifetime sheet in the neighbourhood of the focal plane. Pixels affected by sparse sampling noise are evident but the effect is not as strong as in intensity mode.

In Fig. 12 (b) 4 low-DCR SPADs are activated, with little evidence of sparse sampling noise. A uniform lifetime of approximately 1.6ns is obtained in areas far from the focus. Near the focus, pile-up causes reduction of the measured lifetime to less than 1ns. The effect of spatial sampling noise has disappeared but pile-up is now significant. The blue regions indicate lower than expected lifetimes.

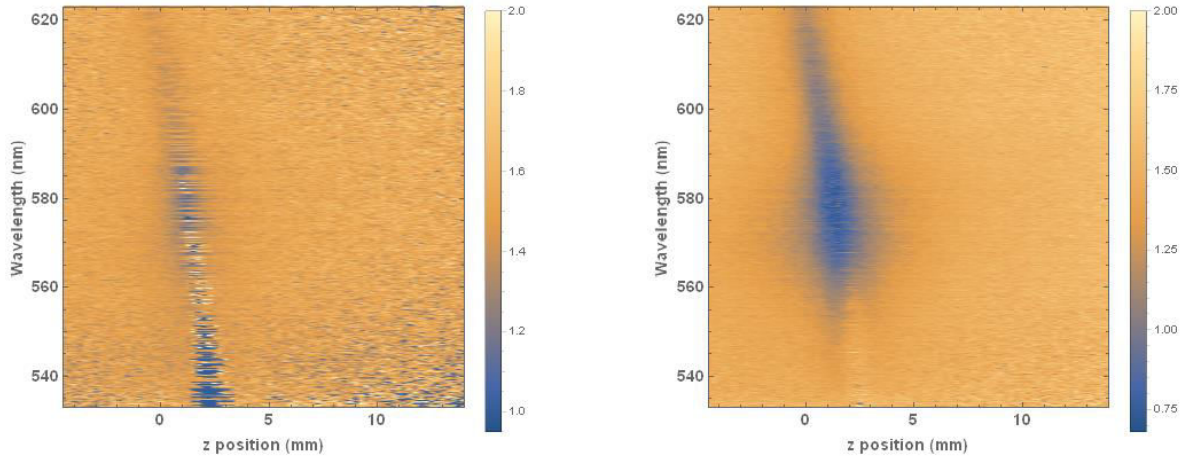

Figure 12. Rhodamine fluorescence lifetime detected in histogramming mode as a function of distance from the focal plane of the spectrometer lens. Excitation wavelength = 532nm. Colour bar denotes lifetime scale in nanoseconds. (a) 1 lowest-DCR SPAD activated. Some evidence of sparse sampling noise. (b) 4 lowest-DCR SPADs activated, with little evidence of sparse sampling noise. Uniform lifetime of approximately 1.6ns in areas far from the focus. Near the focus, pile-up causes reduction of the measured lifetime to less than 1ns.

In Fig. 13 we plot (a) theoretical pile-up reduced lifetime as a function of summed TCSPC counts based on Eq. (2) and (b) experimental results at 512 wavelengths x 75 spatial positions in the vicinity of the focus. Theory and experiment are in broad agreement.

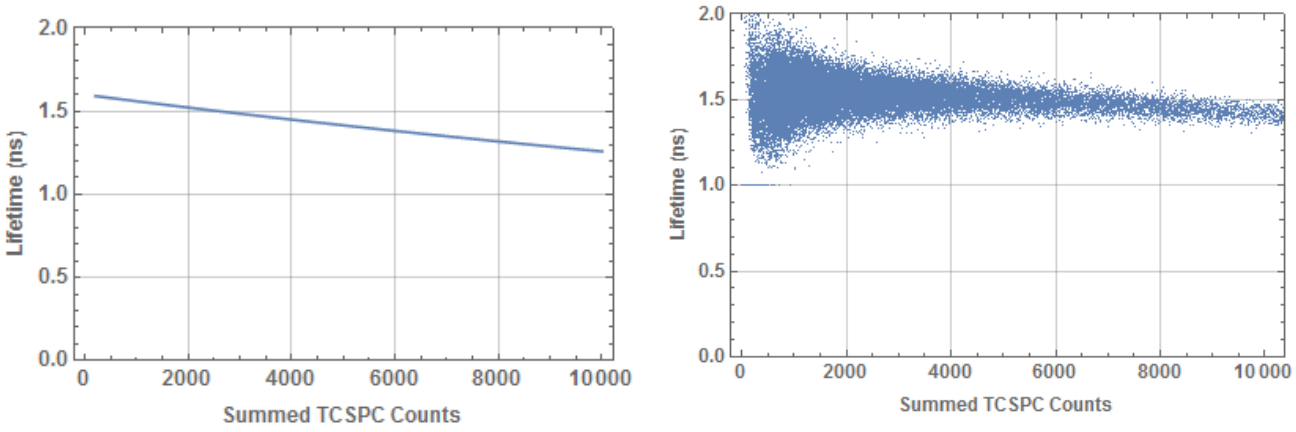

(a) (b)

Figure 13 Lifetime measured as a function of summed TCSPC counts at 512 wavelengths and 75 spatial positions in the vicinity of the focus. (a) Theoretical lifetime based on classical pile-up model, (b) Activation Matrix C experimental measurements (1 SPAD activated per pixel).

7. CONCLUSION

Programmable SPAD activation in CMOS SPAD sensors offers significant benefits in terms of dealing with various types of signal distortion, facilitating trade-offs among dark count noise, spatial sampling noise, distortions arising from optical aberrations and pile-up. In this paper we have explored such trade-offs in a high-throughput line sensor intended for spectroscopy and bio-medical imaging applications. The impact of distortions and various choices of SPAD activation matrix were explored in both single photon counting and time-correlated single photon counting modes. The problem and origins of sparse spatial sampling noise has been highlighted, and one SPAD activation algorithm has been proposed which represents a reasonable compromise in terms of optimising signal-to-noise ratios overall.

ACKNOWLEDGEMENTS

We would like to thank the Engineering and Physical Sciences Research Council (EPSRC, United Kingdom) Interdisciplinary Research Collaboration (grant number EP/K03197X/1 - Proteus) for funding this work. We would also like to thank EPSRC and MRC Centre for Doctoral Training in Optical Medical Imaging, OPTIMA, (grant number EP/L016559/1). We would also like to thank ST Microelectronics, Imaging Division, Edinburgh, for their generous support in manufacturing of the CMOS SPAD line sensors.

REFERENCES

[1] Krstajić, N., Levitt, J., Poland, S., Ameer-Beg, S. and Henderson, R., "256 × 2 SPAD line sensor for time resolved fluorescence spectroscopy," Opt. Express 23(5), 5653 (2015).

[2] Becker, W., [Advanced Time-Correlated Single Photon Counting Applications], Springer International Publishing, Cham (2015).

[3] Nissinen, I., Nissinen, J., Keränen, P. and Kostamovaara, J., "On the effects of the time gate position and width on the signal-to-noise ratio for detection of Raman spectrum in a time-gated CMOS single-photon avalanche diode based sensor," Sensors Actuators B Chem. 241, 1145–1152 (2017).

[4] Palubiak, D. P. and Deen, M. J., "CMOS SPADs: Design Issues and Research Challenges for Detectors, Circuits, and Arrays," IEEE J. Sel. Top. Quantum Electron. 20(6), 409–426 (2014).

[5] Erdogan, A. T., Walker, R., Finlayson, N., Krstajic, N., Williams, G. O. S. and Henderson, R. K., "A 16.5 giga events/s 1024 × 8 SPAD line sensor with per-pixel zoomable 50ps-6.4ns/bin histogramming TDC," 2017 Symp. VLSI Circuits, C292–C293, IEEE (2017).

[6] Pancheri, L. and Stoppa, D., “A SPAD-based pixel linear array for high-speed time-gated fluorescence lifetime imaging,” 2009 Proc. ESSCIRC, 428–431, IEEE (2009).

[7] Maruyama, Y., Blacksberg, J. and Charbon, E., “A 1024$\,\times\,$8, 700-ps Time-Gated SPAD Line Sensor for Planetary Surface Exploration With Laser Raman Spectroscopy and LIBS,” IEEE J. Solid-State Circuits 49(1), 179–189 (2014).

[8] Braga, L. H. C., Perenzoni, M. and Stoppa, D., “Effects of DCR, PDE and saturation on the energy resolution of digital SiPMs for PET,” 2013 IEEE Nucl. Sci. Symp. Med. Imaging Conf. (2013 NSS/MIC), 1–4, IEEE (2013).